High-speed synchrotron X-ray imaging of glass foaming and thermal conductivity simulation

Østergaard, Martin B.; Zhang, Manlin; Shen, Xiaomei; Petersen, Rasmus R.; König, Jakob; Lee, Peter D.; Yue, Yuanzheng; Cai, Biao

Link to publication on Research at Birmingham portal

4D Synchrotron X-ray Imaging of Glass Foaming and Thermal Conductivity Simulation

Martin B. Østergaard[1], Manlin Zhang[2], Xiaomei Shen[2], Rasmus R. Petersen[1], Jakob König[3], Peter D. Lee[4,5,*], Yuanzheng Yue[1,*], Biao Cai[2*]

[1]Department of Chemistry and Bioscience, Aalborg University, DK-9220 Aalborg East, Denmark

[2]School of Metallurgy and Materials, University of Birmingham, Birmingham B15 2TT, UK

[3]Advanced Materials Department, Jožef Stefan Institute, SI-1000 Ljubljana, Slovenia

[4]Department of Mechanical Engineering, University College London, Torrington Place, London WC1E 7JE, UK

[5]Research Complex at Harwell, RAL, Didcot, OX11 0FA, UK

[*]Corresponding authors. E-mails: P.D.L. peter.lee@ucl.ac.uk, Y.-Z.Y. yy@bio.aau.dk, and B.C. b.cai@bham.ac.uk

Abstract

Glass foams are attractive thermal insulation materials, thus, the thermal conductivity (λ) is crucial for their performance. Understanding the foaming process can be of great help for the optimization of process trajectory. Here, we applied high-speed synchrotron X-ray tomography to investigate the change in pore structure during the foaming process and reconstructed the foam structures and porosities. The results can provide guidance for the manufacturing of glass foams. The recorded 3D pore structures were used to determine λ of glass foams with the same chemical composition. We used the simulated λ to develop a new analytical model to predict the porosity dependence of λ. The λ values predicted by the new model are in excellent agreement with the experimental data collected from the literatures, with an average error of only 0.7%, which performs better than models proposed in the literature.

Keywords: Glass foam; Thermal conductivity; 3D image analysis; Simulation; Porosity

1. Introduction

Glass foams are attractive insulation materials as their high porosity results in a low thermal conductivity, thus, a good insulating ability, in combination with load-bearing capability, resistance to humidity, very long lifespan, recyclability, and non-combustibility [1]. As the thermal conductivity is important for glass foams when used as insulation materials, it is necessary to gain knowledge of thermal conductivity of glass foams and other porous materials. Focusing on glass foams, the thermal conductivity decreases roughly linearly with decreasing foam density and increasing porosity [2–4]. As the porosity increases, the contributions of each phase and pore structure become increasingly important. The thermal conductivity of highly porous glass foams is, therefore, greatly dependent on the contribution of the glass phase [5] and its susceptibility to crystallization or its crystal content from foaming residues [6,7], the composition of the gaseous phase in the pores [8], the porosity type (open or closed) and the pore structure (pore size and thickness of struts and walls) [2,3,7,9–11].

In order to obtain a high porosity, it is necessary to optimize the glass foaming process. The most common foaming method is a chemical approach, where glass powder is mixed with foaming agent(s) that generates gas during heating, and the gas expands the viscous glass [1]. *Ex situ* measurements have been used to determine, e.g., the optimum heating rate [12–14], maximum foaming temperature [15–19], isothermal heating duration [2,13,20], and foaming agent content [21,22]. The drawback of these measurements is the inaccuracy in obtaining the real optimum temperatures, as especially the maximum foaming temperature is usually determined in steps of 25–50 °C. In contrast, the hot stage microscopy can be used to measure the change in size *in situ* as the sample expands during heating [23–27]. However, this still lacks the possibility of investigating any differences in the pore structure.

X-ray tomography can provide information on the porous structure with great spatial visualization and quantitative structural details [3,10,17,28,29]. In previous studies, all analyses were carried out on glass foams after cooling, and thus, the dynamic changes in the porous structure cannot be understood, yet some insight to the development of the structure can be obtained from *ex situ* measurements. Changes in the macro- and microstructure can be monitored *in situ* using high-speed synchrotron X-ray tomography while changing external conditions, e.g., during heating or pressing. The changes in the structure were monitored during liquid to solid transformations of metals [30,31], outgassing of volcanic glass [32], heating of dough during breadmaking [33], melting of waste glass [34], and foaming of metals [35].

In this study, we use high-speed synchrotron X-ray tomography to obtain tomograms of a glass foam during the foaming process, and hence, monitor the expansion. Using this technique, we can reconstruct the macroscopic structure of the glass foam at different temperatures and acquire the changes in pore size and porosity during heating. Image-based simulations of the macroscopic structure are used to determine the thermal conductivity of the glass foams. This allows us to model the porosity dependence of the thermal conductivity of glass foams.

2. Experimental

2.1. Sample Preparation

Cathode ray tube (CRT) panel glass powder was mixed with 2.50 mol% carbon and 1.99 mol% Mn_3O_4 as described in Ref. [25]. A pellet of the powder mixture (13 mg) was uniaxially pressed by hand to form a cylinder with a diameter of 1 mm and the height of approx. 4 mm. The pellet was transferred to an alumina crucible that was inserted into a radiation furnace for foaming.

2.2 Foaming and *in situ* tomography

The integrated radiation furnace (described in Ref. [36]) was used at beamline I12 (Diamond Light Source, United Kingdom) to perform *in situ* synchrotron tomographic foaming experiments. The sample was rapidly heated to 585 °C and further heated to 840 °C at 5 °C min^{-1}. Before heating, the chamber was flushed with nitrogen, and a constant nitrogen flow (approx. 5 mL min^{-1}) was introduced during heating to ensure an inert atmosphere. A 53 keV monochromatic X-ray beam was used, and the radiographs were acquired using a PCO.edge camera at camera module 3 [37]. 1000 radiographs were obtained over 180° with an exposure time of 5 ms per radiograph.

2.3 Image analysis

The radiographs were utilized to reconstruct the structure of the glass foam during heating with a voxel size of 3.2 μm voxel^{-1}. The images were processed and analyzed using Avizo and ImageJ software. To ensure identical procedure for segmentation of all images, we applied a machine-learning-based image processing plug-in in ImageJ (Trainable Weka Segmentation [38]). Pixels were manually assigned to a distinct phase (solid or gas) through the trainable Weka Segmentation creating a model (or classifier) that was then applied to all images. The porosity was determined as the ratio between the volume of pores and the total volume. The pore thickness at different temperatures during heating was evaluated using the BoneJ plug-in [39] in ImageJ.

2.4 Simulation of thermal conductivity

The room temperature thermal conductivity (λ) was simulated for macrostructures appearing at several temperature stages, thus, various porosities, using the "Thermal conductivity experiment simulation" built-in module in the Avizo software, which is based on Fourier's law. The input and

output temperatures were set to 373 K and 298 K, respectively. The λ of the solid and gas phases wad set to 0.925 W m^{-1} K^{-1} [2] (as calculated by the Choudhary and Potter model [40]) and 0 W m^{-1} K^{-1} for insulating gas phase (i.e., vacuum), 0.026 W m^{-1} K^{-1} for air gas phase [41], and 0.016 W m^{-1} K^{-1} for CO_2 gas phase [42], respectively. Three series of simulations were carried out using the three different options for the gas phase. The first series considered only the glass phase as the gas phase is considered a thermal insulator, whereas the second and third series considered both the glass and the gas phases with the gas phase being either air or CO_2.

3. Results and discussion

The reconstructions of the glass foams at different temperatures during heating show significant changes in the porous structure (Fig. 1). At 776 °C, an almost completely bulk sample is shown with only minor degree of pores, but with increasing temperature, the number of pores increase until a temperature around 803 °C is reached. Further heating up to 835 °C leads to a gradual increase in the pore size. The change in the measure pore size is shown in Fig. 2. The significant increase in the porosity at temperatures below 800 °C (porosity increases from 5 to 60 %) is clearly caused by nucleation of new pores, as their size do not change significantly (Fig. 2), supported by a recent foaming study of metals [35]. Recently it was observed in glass foam light-weight aggregates that the porosity increases without any change in pore size before reaching a porosity around 60 %. The higher porosities at the later stage of heating is thereafter caused by an increase in pore size [11]. The porosity increase is also visualized in the reconstructed 3D structures in Fig. 3, where the thickness increases due to the larger pore size. Above 800 °C, the pore size increases, resulting in a further increase in the porosity (60–90 %) owing to the following factors. Firstly, the pressure inside pores is higher than that in the atmosphere, and hence, the melt expands. As the foaming agent oxidization progresses, more gas

is evolved, leading to a larger expansion [24]. At the same time, increasing temperature lowers the melt viscosity, thus decreasing the opposing force for the expansion of the pores. Secondly, the initial pores are mainly spherical [18] which minimizes the surface energy. However, as the melt viscosity decreases, the pore walls become thinner and eventually break, triggering the coalescence process that increases the pore size and creates non-spherical pores [43]. The coalescence also provokes incorporation of small pores into large pores, and thereby the small pores disappear [44]. The non-spherical shape of the pores enhances the pore coalescence [45]. The non-spherical pores would transform into a sphere, but there is not sufficient time available as pore walls continuously break and small pores diffuse into the larger pores, thus, the pore shape remains polyhedral. Fig. 4 shows how two non-spherical large pores combine into one due to the rupture of the pore wall (illustrated by the red rectangle).
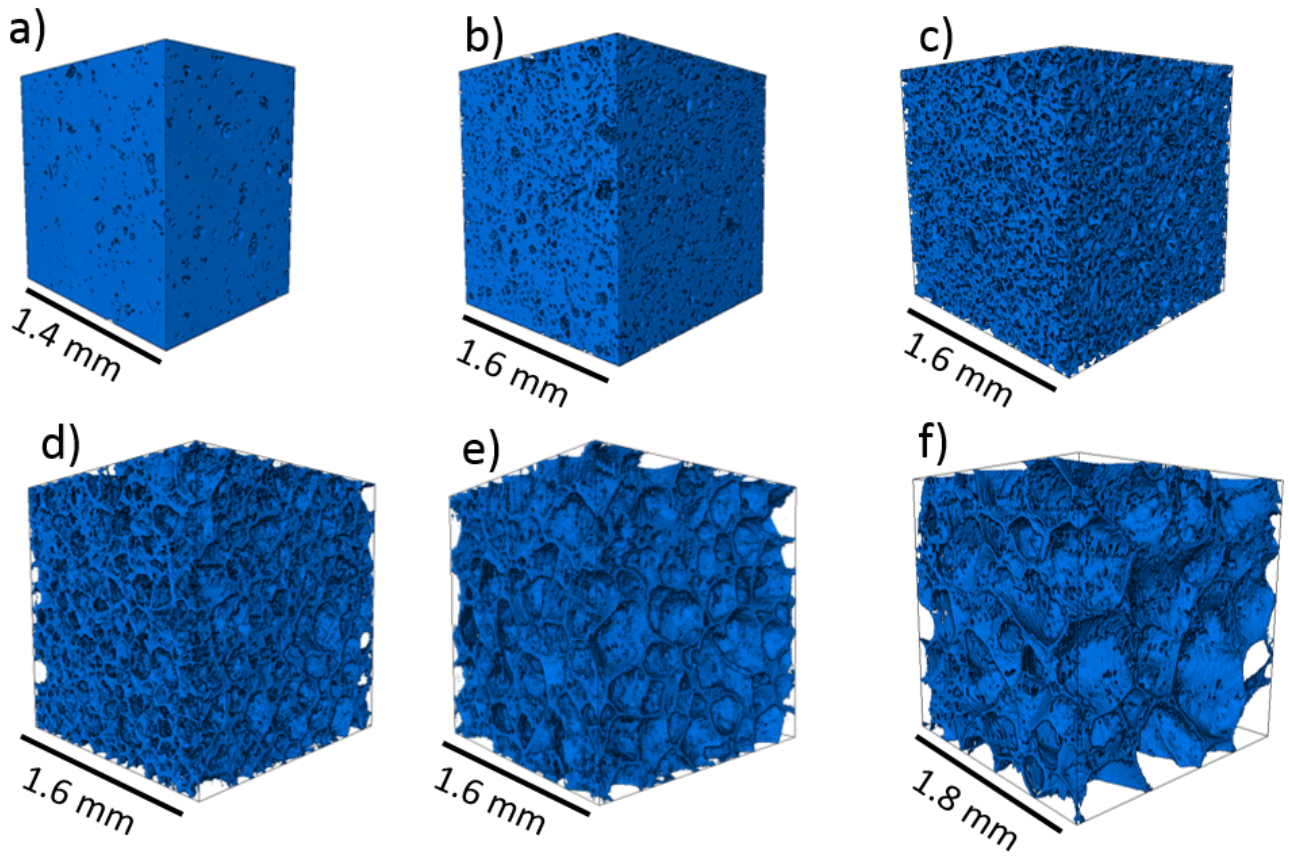
Fig. 1. 3D reconstructions of glass foams at different temperatures during heating, a) 776 °C, b) 787 °C, c) 803 °C, d) 811 °C, e) 819 °C, and f) 835 °C.
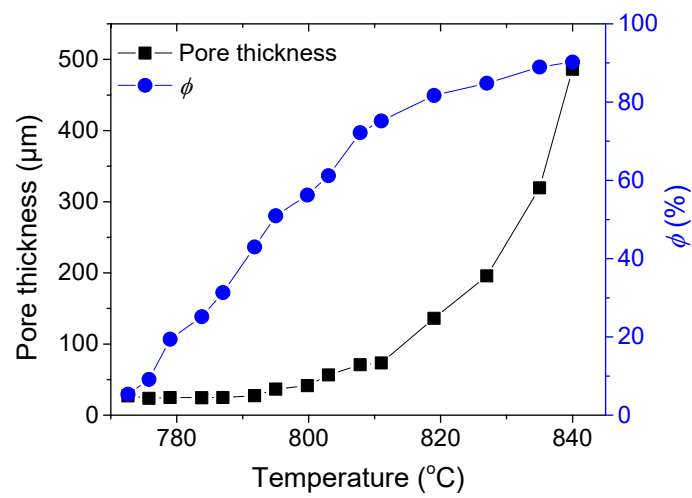
Fig. 2. Changing of the pore size (measured as pore thickness) and porosity (ϕ) during heating.
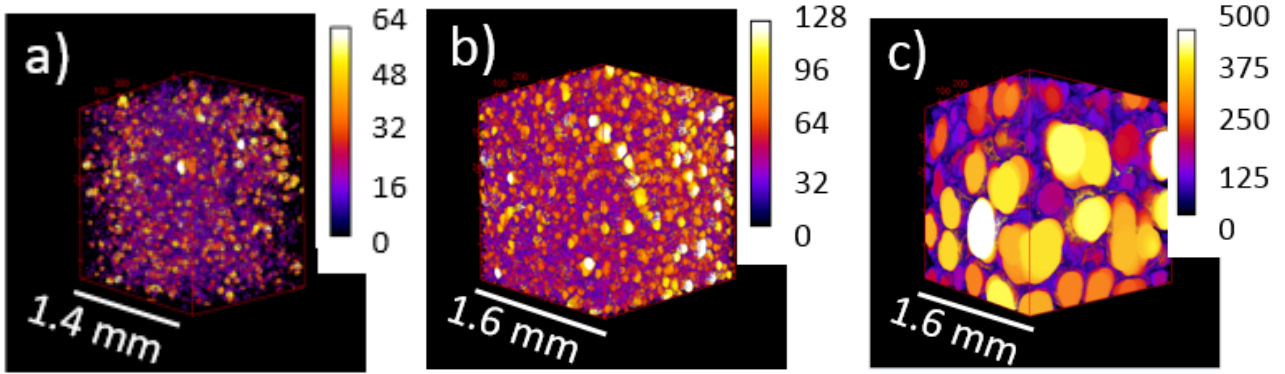
Fig. 3. 3D rendering of the thickness of the pores showing the changing pore size with increasing temperature at a) 756 °C, b) 800 °C, and c) 827 °C. The color scale shows the pore sizes (diameter) in µm.
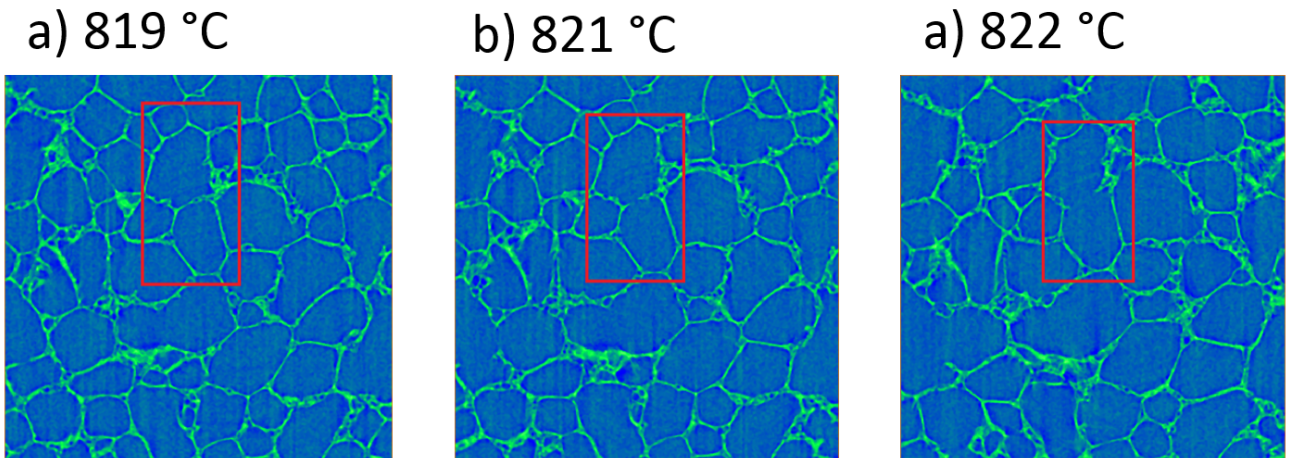
Fig. 4. Coalescence of the pores during heating (marked with a rectangle). a) two pores separated by a pore wall, b) beginning of the rupture in the pore wall, and c) complete rupture of the pore wall and a combined larger pore with irregular shape.

The porosity dependence of the thermal conductivity (λ) is simulated using image based simulation for glass foams based on 3D pore structures (Fig. 5). When considering the gas phase as a thermal insulator, the heat is only transported through the glass phase (Fig. 5a), whereas when considering the actual gas phase the heat is transported through both gas and solid phases (Fig. 5b). Hence, the glass skeleton is only visible in the simulation when the pores are considered as an insulator. Simulations of λ throughout the porosity range of 5–90 % are carried out for the three cases taking into consideration of different gaseous contributions, i.e., 0, 0.016, and 0.026 W m^{-1} K^{-1} for the thermal insulator, CO_2, and air, respectively (Fig. 6). The thermal conductivity of the solid phase (λ_s) is 0.925 W m^{-1} K^{-1} [2]. The gaseous contribution is insignificant at low porosity as the dominant phase in the sample is glass with two orders of magnitude higher thermal conductivity. However, with increasing porosity, the difference in λ gets more pronounced, displaying an increase in λ in the order of air > CO_2 > insulating, agreeing with previous experimental findings [8]. This indicates the importance of considering the gas phase contribution into simulations.
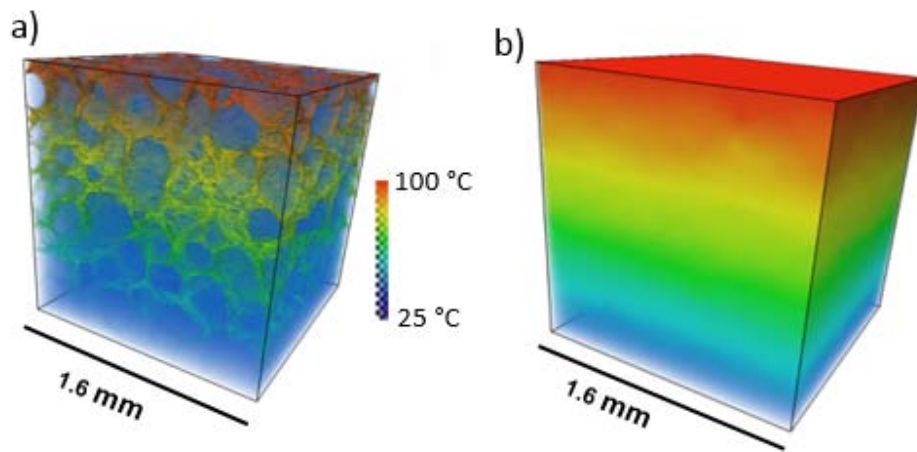

Fig. 5. Simulated heat gradient through a glass foam with a) the gas phase considered an insulator and b) the gas phase included as air.
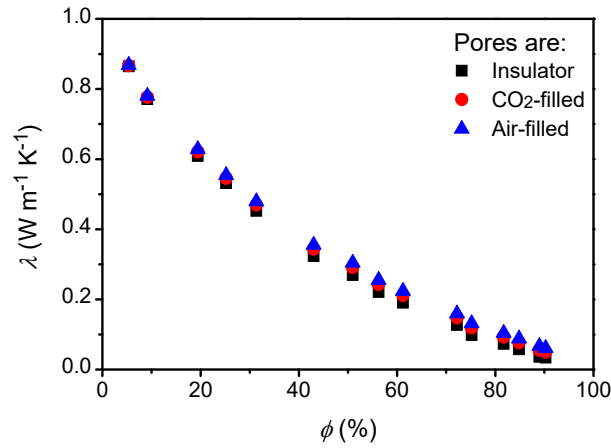
Fig. 6. Simulation of the thermal conductivity (λ) as a function of porosity (ϕ) and gas phase for a glass foams with glass conductivity of 0.925 W m^{-1} K^{-1} (pores as thermal insulator or ones filled with CO_2-filled or air-filled). The pore structure changes throughout the increase in porosity, though, are identical among the gas comparison at same porosity.

The simulated λ values at different porosities are compared to reported experimental values for the glass foams derived from CRT panel glass [2,5,8,10,20,22,46] in Fig. 7. We note that in the literature the porosities in some cases are not reported, and we therefore calculate it using the bulk density values or using a bulk density (ρ_s) of 2.76 g cm^{-3} [24]. As expected the simulated curves for real gas phases (CO_2 or air) describe the experimental values better than the simulated curve, where the gas phase is assumed to be a thermal insulator. The majority of the experimental data are surrounded about the lines for air and CO_2, probably due to the mixture of gases (CO_2, O_2, CO, Ar, and N_2) present in the pores. Therefore, the gas phase is a crucial parameter for simulating λ. Some reported values are higher than the simulated values, and this can be due to crystal residues from foaming agents in the solid phase [6]

or a difference in the pore structure, e.g., in pore size [9–11]. Both differences increase the contribution of the solid phase to the effective thermal conductivity.
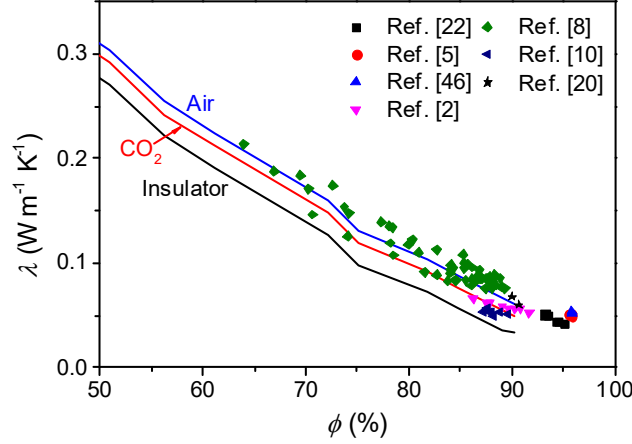
Fig. 7. Comparison of the simulated thermal conductivity (λ) and experimental λ values in glass foams based on CRT panel glass from the literature.

The simulated λ values are in good agreement with the experimental ones from the literature when exceeding a porosity of 60 % (Fig. 7). Due to a lack of data for the lower porosity region, we fit a linear equation to the simulated values for porosities of >50 %. This fitting is done for the case of the air-filled pores. The porosity dependence of λ is expressed by the fit of Eq. 1.

$$\lambda = -0.01 + (1 - \phi)0.6 \tag{1}$$

Considering the λ-values of the solid and gaseous phase, Eq. 1 can be converted to Eq. 2 by describing the first term as the gaseous contribution and the second term as the solid contribution:

$$\lambda = \lambda_g(\phi - 1) + \frac{2}{3}(1 - \phi)\lambda_s \tag{2}$$

where λ, λ_g, and λ_s is the thermal conductivities of the foam, the gas, and the solid, respectively, and ϕ is the porosity of the glass foam.

To compare Eq. 2 with the existing models regarding the quality of the description of the porosity dependence of the λ value for porous materials, we test four other analytic models which has been widely used to simulate the thermal conductivity, namely, the Russell [47], the Landauer [48], the Schuetz-Glicksman [49], and the Doherty-Hurd-Lestor [50] models against the same simulated values by our image based simulation (Fig. 8). We note that many more models exist based on theoretical or semi-empirical work [51]. Among these models, the Schuetz-Glicksman (Eq. 5) [49] and the Doherty-Hurd-Lestor (Eq. 7) [50] models are similar depending on the K value in the Schuetz-Glicksman model. Both are in good agreement with Eq. 2, yet different from Eq. 2, in which we account for the porosity in both gas and solid contribution terms in contrast to the previous models. These four models are, as Eq. 2, based on the porosity and the solid and the gas phase conductions. The four existing models treat the conduction through solid (λ_s) and gas (λ_g) as decoupled. We use the same values for λ_s and λ_g as described earlier (λ_s=0.925 W m^{-1} K^{-1} and λ_g=0.016 W m^{-1} K^{-1}). In other words, we assume there is pure CO_2 in the pores and the solid matrix composes of CRT panel glass, which are used in our calculation based on a model developed by Choudhary and Potter [40]. The λ_s of a glass obtained by remelting CRT panel glass is reported to be 0.866 W m^{-1} K^{-1}, while that of a CRT panel glass remelted with 4 wt% MnO_2 is 0.932 W m^{-1} K^{-1} [6]. Therefore, the λ of the solid matrix phase (λ_s=0.925 W m^{-1} K^{-1}) already includes the contributions from the incorporation of manganese oxide into the glass phase and a low degree of Mn_3O_4 or MnO crystal residues that can be found in the glass matrix [2].

The Russell model [47] is an analytical model based on gas-filled cubes (Eq. 3) describing the thermal conductivity of a foam:

$$\lambda_f = \frac{\lambda_s(\lambda_s + \phi^{\frac{2}{3}}(\lambda_g - \lambda_s))}{\lambda_s + (\lambda_g - \lambda_s)(\phi^{\frac{2}{3}} - \phi)} \tag{3}$$

where λ_s and λ_g are the solid and gas conductivity, respectively, and ϕ is the porosity. In contrast, the Landauer model (Eq. 4) [48] describes λ of porous materials based on the assumption that two media are randomly dispersed:

$$\lambda_f = \frac{1}{4}[(\lambda_g(3\phi - 1)) + \lambda_s(3\phi_s - 1) + ([\lambda_g(3\phi - 1) + \lambda_s(3\phi_s - 1)]^2 + 8\lambda_s\lambda_g)^{\frac{1}{2}}] \tag{4}$$

where φ_s is the solidity $(1 - \phi)$, i.e., fraction of solid in the foam. The Schuetz-Glicksman model (Eq. 5) [49] is a simplified expression of the Russell model at low densities:

$$\lambda_f = \lambda_g + K(1 - \phi)\lambda_s \tag{5}$$

$$K = \tau(\frac{2}{3} - \frac{f_s}{3}) \tag{6}$$

where τ is the tortuosity factor and f_s is the fraction of the solid occurring in the strut. When $f_s = 0$, all solid is the entire wall of pores, whereas for $f_s = 1$, all solid is in the struts. The factor of $(2/3 - f_s/3)$ represents the fraction of the solid aligned parallel to the heat flow. The K-factor was estimated to be close to 0.34 for glass foams prepared from CRT panel glass and MnO_2 [2]. The Doherty-Hurd-Lestor model (Eq. 7) is identical to the Schuetz-Glicksman model when K=2/3.

$$\lambda_f = \lambda_g + \frac{2}{3}(1 - \phi)\lambda_s \tag{7}$$

The simulated λ is well described by the new model (Eq. 2) for porosities of >40 %, despite a slight overestimation (Fig. 8). The Landauer model slightly overestimates the simulated λ at porosities of <40 % and greatly underestimates the simulated λ at porosities of >40 %. The latter is due to

underestimation of the solid thermal conduction. The Russell model generally overestimates the simulated λ throughout the entire porosity range. The Schuetz-Glicksmann model slightly underestimates the simulated λ at porosities of >80 %, but it is useless at lower porosity (<80%). Finally, the Doherty-Hurd-Lestor model is almost parallel to Eq. 2 with a larger overestimation at porosities >40 %, while heavily underestimates low porosity glass foams. Thus, a combined model of the Landauer model at low porosity (<40 %) and Eq. 2 at high porosity (>40 %) can be used to describe the porosity dependence of λ in the entire porosity range.
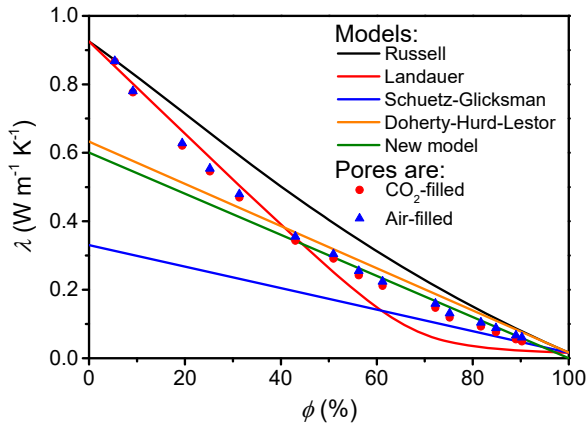
Fig. 8. Comparison of the five models' ability to describe the simulated thermal conductivity (λ) based on the porosity (ϕ). The λ values used in the models for solid and gas are 0.925 W m^{-1} K^{-1} and 0.016 W m^{-1} K^{-1}, respectively.

The experimental λ data used in Fig. 7 are plotted to compare the four different models (Fig. 9). In all reported studies, the porosity, glass type, and foaming agent type are required inputs for predicting λ. As described earlier, densities are utilized to calculate porosities. Here, we used only the CRT panel glass derived glass foams for simulations, and thus we can maintain the same ρ_s and λ_s. However, we

ignore the difference in the type of the gas phase (most relevant are CO_2, CO, O_2, N_2, Ar, and their mixtures), and consider CO_2-filled pores in the model.

There are no reports for λ of glass foams with porosities <60 % (Fig. 9). Therefore, the interesting region is of highly porous glass foams, since high porosity results in lower λ, which is important for the use of glass foams as thermal insulation material. As seen in the inset of Fig. 9, the new model (Eq. 2) describes the λ trend much better than the four other models. Though, the Schuetz-Glicksman model is to give the best fit for Ref. [10], while the Russell and Doherty-Hurd-Lestor models for Refs. [5,46]. The Landauer model is not suitable for the highly porous glass foams. Based on this comparison, an empirical model (Eq.2) based on simulated λ values of glass foam structures depicts the thermal conductivity of glass foams better than the theoretical models.
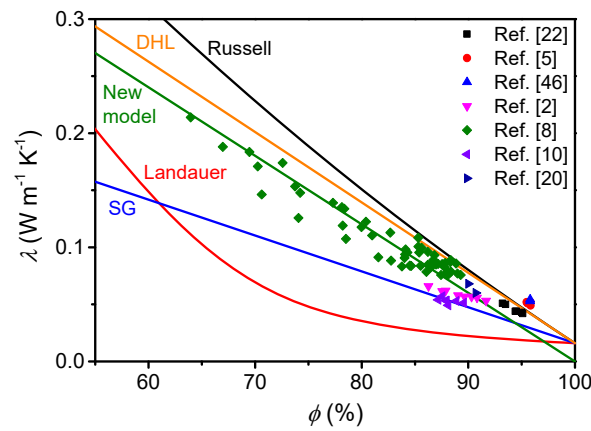
Fig. 9. Comparison of experimental thermal conductivities (λ) of glass foams based on CRT panel glass from various studies described as function of porosity (ϕ) and the fits by the Russell, the Landauer, the Schuetz-Glicksman (SG), Doherty-Hurd-Lestor (DHL), and the new model (Eq. 2).

Glass foams based on CRT panel glass were used for the initial comparison of the models since these are similar to the simulated glass foams. To make a broader comparison of the models, we model the ϕ dependence of λ for glass foams based on different types of glasses and containing different gases and compare them with their experimental λ values from the literature (Fig. 10a). The comparison was made for the porosity > 40 %. Experimental λ data are taken from Refs. [2–5,8,10,20,22,27,46,52–55], and the average difference between the modelled and experimental values is shown in Fig. 10b. In order to model the ϕ dependence of λ, we have made the following assumptions regarding λ_s and λ_g. The λ_s contributions of CRT panel glass, funnel glass, and soda-lime silica glasses (window, flat, bottle) are 0.925 [2], 1.046 [56], and 1.1 W m^{-1} K^{-1} [3], respectively. For glass mixtures, we presume a linear relation between the λ_s and the fraction of the specific glass, and thereby calculate the approximate λ_s. λ_g of CO_2, O_2, N_2, Ar (mixture with CO_2), N_2 (mixture with CO_2), H_2O, and SO_2 are 0.016 [42], 0.026 [41], 0.026 [41], 0.016 [8], 0.023 [8], 0.019 [57], and 0.0099 W m^{-1} K^{-1} [58], respectively. The gas might be a multicomponent phase as reported previously [5,8], but to predict λ, we assume one-phase gas compositions unless λ_g of the multicomponent gas phase is reported. For simplicity, we do not consider the ratio of the closed and the open pores in modeling, but assume 100 % closed pores filled with the gas evolved during foaming, e.g., CO_2 released from carbonaceous substances, N_2 from TiN, and O_2 from MnO_2. In the case of lack of porosity data, we acquire data by calculations based on the foam density and bulk solid density, where the solid density is 2.76 [8], 3.00 [59], and 2.48 g cm^{-3} [60] for CRT panel glass, CRT funnel glass, and soda-lime silica glasses, respectively.

To illustrate the difference between the new model (Eq. 2) and the four existing models analyzed in this paper, we plot the difference in the experimental and the modelled λ data against ϕ (Fig. 10). Eq. 2

is, in general, closer to the experimental values (Fig. 10a). In contrast, the Russell model underestimates, whereas the Landauer and Schuetz-Glicksman models overestimate λ. Eq. 8 describes the difference between the modeled and the experimental λ values.

$$Difference = \frac{\lambda_{exp} - \lambda_{model}}{\lambda_{exp}} \cdot 100 \qquad (8)$$

Where λ_{exp} and λ_{model} are the experimental and modelled thermal conductivity, respectively. The average difference implies that the Russell model overestimates λ by 31 % (as the experimental value is 31 % lower than the predicted) and the Doherty-Hurd-Lestor overestimates by 24 %, while both the Landauer model and the Schuetz-Glicksman models underestimate λ by 60 % and 26 %, respectively. In contrast, the new model only exhibits a difference of 0.7 % on average for glass foams with porosity >40 % (Fig. 10b). The comparison suggests that Eq. 2 performs better than other models in terms of prediction of λ of glass foams.
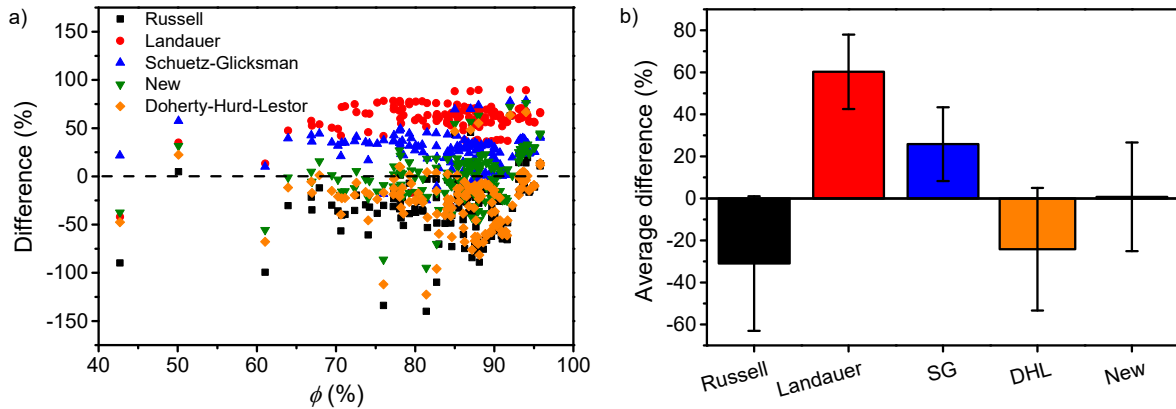
Fig. 10. a) Difference (Eq. 8) in the thermal conductivity (λ) when comparing calculated and experimental values from the literature at different porosities (ϕ) and b) average difference in thermal

conductivity for the Russell, Landauer, Schuetz-Glicksman (SG), Doherty-Hurd-Lestor (DHL), and new (Eq. 2) models.

4. Conclusions

The foaming of a glass melt is monitored using the synchrotron X-ray tomography. The developing and growing pores cause an increase in the sample volume due to the gas formation, thus, the porosity of the sample increases. The initial increase in the porosity is caused by formation of new small pores, while at higher temperatures the pores start to expand due to high pressure. The highest porosity determined for the investigated glass foam is 90.2 %. Based on the 3D reconstructions of the glass foam structures at different temperatures, the thermal conductivity (λ) is simulated for each structure using an image-based numerical technique. The simulated λ decreases from approx. 0.86 W m^{-1} K^{-1} at a porosity of 6% to 0.03–0.06 W m^{-1} K^{-1} at a porosity of 90 %, depending on pores being either insulators, CO_2-filled or air-filled, with the insulating pores resulting in the lowest thermal conductivity.

By comparing the simulated λ with the experimental data from the literature, the gas phase is found to be crucial for the simulation of the λ. Finally, we develop a new empirical model (Eq. 2) to describe the porosity dependence of λ of glass foams (and plausibly other porous materials) as a function of porosity for the case of $\phi > 40$ %. The new model exhibits an average difference of only 0.7 % between the modeled and experimentally obtained λ values, compared to the average difference of 26–60 % achieved by the four considered analytical models.

References

[1]   G. Scarinci, G. Brusatin, E. Bernardo, Glass foams, in: M. Scheffler, P. Colombo (Eds.), Cell. Ceram. Struct. Manuf. Prop. Appl., Wiley-VCH Verlag GmbH & Co KGaA, Weinheim, 2005: pp. 158–176.

[2]   R.R. Petersen, J. König, Y. Yue, The mechanism of foaming and thermal conductivity of glasses foamed with MnO_2, J. Non. Cryst. Solids. 425 (2015) 74–82.

[3]   J.P. Wu, A.R. Boccaccini, P.D. Lee, R.D. Rawlings, Thermal and mechanical properties of a foamed glass-ceramic material produced from silicate wastes, Proc. Eighth Eur. Soc. Glas. Sci. Technol. Conf. Glas. Technol. Eur. J. Glas. Sci. Technol. A. 48 (2007) 133–141.

[4]   F. Méar, P. Yot, R. Viennois, M. Ribes, Mechanical behaviour and thermal and electrical properties of foam glass, Ceram. Int. 33 (2007) 543–550.

[5]   J. König, R.R. Petersen, N. Iversen, Y. Yue, Suppressing the effect of cullet composition on the formation and properties of foamed glass, Ceram. Int. 44 (2018) 11143–11150.

[6]   M.B. Østergaard, R.R. Petersen, J. König, H. Johra, Y. Yue, Influence of foaming agents on

thermal conductivity of the CRT panel glass, J. Non. Cryst. Solids. 465 (2017) 59–64.

[7]   Y.A. Spiridonov, L.A. Orlova, Problems of foam glass production, Glas. Ceram. 60 (2003) 313–315.

[8]   M.B. Østergaard, R.R. Petersen, J. König, M. Bockowski, Y. Yue, Impact of gas composition on thermal conductivity of glass foams prepared via high-pressure sintering, J. Non-Crystalline Solids X. 1 (2019) 100014.

[9]   S. Köse, G. Bayer, Schaumbildung im system altglas-SiC und die eigenschaften derartiger schaumgläser, Glas. Ber. 55 (1982) 151–160.

[10]   M.B. Østergaard, B. Cai, R.R. Petersen, J. König, P.D. Lee, Y. Yue, Impact of pore size on thermal conductivity of glass foams, Mater. Lett. 250 (2019) 72–74.

[11]   C. Arriagada, I. Navarrete, M. Lopez, Understanding the effect of porosity on the mechanical and thermal performance of glass foam lightweight aggregates and the influence of production factors, Constr. Build. Mater. 228 (2019) 116746.

[12]   A. Pokorny, J. Vicenzi, C. Pérez Bergmann, Influence of heating rate on the microstructure of glass foams., Waste Manag. Res. 29 (2011) 172–179.

[13]   L. Lakov, K. Toncheva, A. Staneva, Z. Ilcheva, T. Simeonova, Composition , Synthesis and Properties of Color Architecture Building Foam Glass Obtained From Waste Packing Glass, J. Chem. Technol. Metall. 48 (2013) 125–129.

[14]   B. Cicek, L. Esposito, A. Tucci, E. Bernardo, A.R. Boccaccini, P.A. Bingham, Microporous glass ceramics from combination of silicate , borate and phosphate wastes, Adv. Appl. Ceram.

111 (2012) 415–422.

[15]   A.S. Llaudis, M.J.O. Tari, F.J.G. Ten, E. Bernardo, P. Colombo, Foaming of flat glass cullet using Si_3N_4 and MnO_2 powders, Ceram. Int. 35 (2009) 1953–1959.

[16]   V. Ducman, M. Kovacevic, The foaming of waste glass, Key Eng. Mater. 132–136 (1997) 2264–2267.

[17]   J.P. Wu, A.R. Boccaccini, P.D. Lee, M.J. Kershaw, R.D. Rawlings, Glass ceramic foams from coal ash and waste glass : production and characterisation, Adv. Appl. Ceram. 105 (2006) 32–39.

[18]   R. Taurino, I. Lancellotti, L. Barbieri, C. Leonelli, Glass-ceramic foams from borosilicate glass waste, Int. J. Appl. Glas. Sci. 5 (2014) 136–145.

[19]   H.R. Fernandes, F. Andreola, L. Barbieri, I. Lancellotti, M.J. Pascual, J.M.F. Ferreira, The use of egg shells to produce Cathode Ray Tube (CRT) glass foams, Ceram. Int. 39 (2013) 9071–9078.

[20]   E. Bernardo, F. Albertini, Glass foams from dismantled cathode ray tubes, Ceram. Int. 32 (2006) 603–608.

[21]   V. Laur, R. Benzerga, R. Lebullenger, L. Le Gendre, G. Lanoë, A. Sharaiha, P. Queffelec, Green foams for microwave absorbing applications: Synthesis and characterization, Mater. Res. Bull. 96 (2017) 100–106.

[22]   J. König, R.R. Petersen, Y. Yue, Fabrication of highly insulating foam glass made from CRT panel glass, Ceram. Int. 41 (2015) 9793–9800.

[23]   R.R. Petersen, J. König, Y. Yue, Evaluation of foaming behavior of glass melts by high-

temperature microscopy, Int. J. Appl. Glas. Sci. 7 (2016) 524–531.

[24]   M.B. Østergaard, R.R. Petersen, J. König, M. Bockowski, Y. Yue, Foam glass obtained through high-pressure sintering, J. Am. Ceram. Soc. 101 (2018) 3917–3923.

[25]   M.B. Østergaard, R.R. Petersen, J. König, Y. Yue, Effect of alkali phosphate content on foaming of CRT panel glass using Mn_3O_4 and carbon as foaming agents, J. Non. Cryst. Solids. 482 (2018) 217–222.

[26]   H.R. Fernandes, D.D. Ferreira, F. Andreola, I. Lancellotti, L. Barbieri, J.M.F. Ferreira, Environmental friendly management of CRT glass by foaming with waste egg shells, calcite or dolomite, Ceram. Int. 40 (2014) 13371–13379.

[27]   D. Hesky, C.G. Aneziris, U. Groß, A. Horn, Water and waterglass mixtures for foam glass production, Ceram. Int. 41 (2015) 12604–12613.

[28]   L. Korat, V. Ducman, A. Legat, B. Mirtič, Characterisation of the pore-forming process in lightweight aggregate based on silica sludge by means of X-ray micro-tomography (micro-CT) and mercury intrusion porosimetry (MIP), Ceram. Int. 39 (2013) 6997–7005.

[29]   V. Ducman, L. Korat, A. Legat, B. Mirtič, X-ray micro-tomography investigation of the foaming process in the system of waste glass-silica mud-MnO_2, Mater. Charact. 86 (2013) 316–321.

[30]   M.A. Azeem, P.D. Lee, A.B. Phillion, S. Karagadde, P. Rockett, R.C. Atwood, L. Courtois, K.M. Rahman, D. Dye, Revealing dendritic pattern formation in Ni, Fe and Co alloys using synchrotron tomography, Acta Mater. 128 (2017) 241–248.

[31]   C.L.A. Leung, S. Marussi, R.C. Atwood, M. Towrie, P.J. Withers, P.D. Lee, In situ X-ray

imaging of defect and molten pool dynamics in laser additive manufacturing, Nat. Commun. 9 (2018) 1–9.

[32] F.W. von Aulock, B.M. Kennedy, A. Maksimenko, F.B. Wadsworth, Y. Lavallée, Outgassing from Open and Closed Magma Foams, Front. Earth Sci. 5 (2017) 1–7.

[33] P. Babin, G. Della Valle, H. Chiron, P. Cloetens, J. Hoszowska, P. Pernot, A.L. Réguerre, L. Salvo, R. Dendievel, Fast X-ray tomography analysis of bubble growth and foam setting during breadmaking, J. Cereal Sci. 43 (2006) 393–397.

[34] A.S. Choi, D.H. Miller, D.M. Immel, F.G. Smith, Investigation of high-level waste glass melting using X-ray computed tomography, Int. J. Appl. Glas. Sci. 8 (2017) 165–176.

[35] F. García-moreno, P.H. Kamm, T.R. Neu, F. Bülk, R. Mokso, C.M. Schlepütz, M. Stampanoni, J. Banhart, Using X-ray tomoscopy to explore the dynamics of foaming metal, Nat. Commun. 10 (2019) 1–9.

[36] B. Cai, S. Karagadde, L. Yuan, T.J. Marrow, T. Connolley, P.D. Lee, In situ synchrotron tomographic quantification of granular and intragranular deformation during semi-solid compression of an equiaxed dendritic Al-Cu alloy, Acta Mater. 76 (2014) 371–380.

[37] M. Drakopoulos, T. Connolley, C. Reinhard, R. Atwood, O. Magdysyuk, N. Vo, M. Hart, L. Connor, B. Humphreys, G. Howell, S. Davies, T. Hill, G. Wilkin, U. Pedersen, A. Foster, N. De Maio, M. Basham, F. Yuan, K. Wanelik, beamlines I12 : the Joint Engineering , Environment and Processing (JEEP) beamline at Diamond Light Source beamlines, J. Synchrotron Radiation2. 22 (15AD) 828–838.

[38] I. Arganda-carreras, V. Kaynig, C. Rueden, K.W. Eliceiri, J. Schindelin, A. Cardona, H.S. Seung, Trainable Weka Segmentation : a machine learning tool for microscopy pixel classification, Bioinformatics. 33 (2017) 2424–2426.

[39] M. Doube, M.M. Klosowski, I. Arganda-Carreras, F.P. Cordelières, R.P. Dougherty, J.S. Jackson, B. Schmid, J.R. Hutchinson, S.J. Shefelbine, BoneJ: Free and extensible bone image analysis in ImageJ, Bone. 47 (2010) 1076–1079.

[40] M.K. Choudhary, R.M. Potter, Heat transfer in glass-forming melts, in: L.D. Pye, A. Montenero, I. Joseph (Eds.), Prop. Glas. Melts, Second, CRC Press, Taylor & Francis, 2005.

[41] E.W. Lemmon, R.T. Jacobsen, Viscosity and thermal conductivity equations for nitrogen, oxygen, argon, and air, Int. J. Thermophys. 25 (2004) 21–69.

[42] A. Michels, J. V Sengers, P.S. van der Gulik, The thermal conductivity of carbon dioxide in the critical region, Physica. 28 (1962) 1216–1237.

[43] A.A. Proussevitch, D.L. Sahagian, V.A. Kutolin, Stability of foams in silicate melts, J. Volcanoogy Geotherm. Res. 59 (1993) 161–178.

[44] F. Méar, P. Yot, M. Ribes, Effects of temperature, reaction time and reducing agent content on the synthesis of macroporous foam glasses from waste funnel glasses, Mater. Lett. 60 (2006) 929–934.

[45] A. Bhakta, E. Ruckenstein, Decay of standing foams: Drainage, coalescence and collapse, Adv. Colloid Interface Sci. 70 (1997) 1–124.

[46] J. König, V. Nemanič, M. Žumer, R.R. Petersen, M.B. Østergaard, Y. Yue, D. Suvorov,

Evaluation of the contributions to the effective thermal conductivity of an open-porous type foam glass, Constr. Build. Mater. 214 (2019) 337–343.

[47] H.W. Russell, Principles of heat flow in porous insulators, J. Am. Ceram. Soc. 18 (1935) 1–5.

[48] R. Landauer, The Electrical Resistance of Binary Metallic Mixtures, J. Appl. Phys. 23 (1952) 779–784.

[49] M. a. Schuetz, L.R. Glicksman, A basic study of heat transfer through foam insulation, J. Cell. Plast. 20 (1984) 114–121.

[50] D.J. Doherty, R. Hurd, G.R. Lestor, The physical properties of rigid polyurethane foams, Chem. Ind. 30 (1962) 1340–1356.

[51] P. Collishaw, J.R.G. Evans, Review An assessment of expressions for the apparent thermal conductivity of cellular materials, J. Mater. Sci. 29 (1994) 2261–2273.

[52] Y. Attila, M. Güden, A. Taşdemirci, Foam glass processing using a polishing glass powder residue, Ceram. Int. 39 (2013) 5869–5877.

[53] C. Vancea, I. Lazău, Glass foam from window panes and bottle glass wastes, Cent. Eur. J. Chem. 12 (2014) 804–811.

[54] D.M.A. Alim, Production and characterization of foam glass from container waste glass, The American University in Cairo, 2009.

[55] M.T. Souza, B.G.O. Maia, L.B. Teixeira, K.G. de Oliveira, A.H.B. Teixeira, A.P. Novaes de Oliveira, Glass foams produced from glass bottles and eggshell wastes, Process Saf. Environ.

Prot. 111 (2017) 60–64.

[56] L. Van Der Tempel, G.P. Melis, T.C. Brandsma, Thermal conductivity of a glass: I. Measurement by the glass–metal contact, Glas. Phys. Chem. 26 (2000) 606–611.

[57] J. V. Sengers, J.T.R. Watson, Improved International Formulations for the Viscosity and Thermal Conductivity of Water Substance, J. Phys. Chem. Ref. Data. 15 (1986) 1291–1314.

[58] E.S. Udoetok, Thermal conductivity of binary mixtures of gases, Front. Heat Mass Transf. 4 (2013) 1–5.

[59] F. Méar, P. Yot, M. Cambon, M. Ribes, The characterization of waste cathode-ray tube glass, Waste Manag. 26 (2006) 1468–1476.

[60] R.R. Petersen, J. König, Y. Yue, The viscosity window of the silicate glass foam production, J. Non. Cryst. Solids. 456 (2017) 49–54.